might exploit a similar strategy based on a very efficient capture mechanism at specialized NMJ sites rich in nidogens, which may function to concentrate TeNT as well as physiological ligands, such as neurotrophic factors, to facilitate their uptake and sorting to axonal transport organelles. At these sites, TeNT in complex with nidogens may interact with surface receptors known to bind nidogens, such as the protein phosphatase LAR (*29*, *30*). This specialized capture mechanism is likely to be indispensable to the host cell, and this enables TeNT to be lethal at extremely low concentrations. Our study suggests that nidogens are prime therapeutic targets for suppressing the uptake of TeNT at the NMJ and its access to the CNS, preventing its lethal effects.

REFERENCES AND NOTES

1. C. Montecucco, *Curr. Top. Microbiol. Immunol.* **195**, 278 (1995).
2. K. Deinhardt *et al.*, *Neuron* **52**, 293–305 (2006).
3. C. Chen, Z. Fu, J. J. P. Kim, J. T. Barbieri, M. R. Baldwin, *J. Biol. Chem.* **284**, 26569–26577 (2009).
4. S. Jayaraman, S. Eswaramoorthy, D. Kumaran, S. Swaminathan, *Proteins* **61**, 288–295 (2005).
5. Q. Chai *et al.*, *Nature* **444**, 1096–1100 (2006).
6. R. Jin, A. Rummel, T. Binz, A. T. Brunger, *Nature* **444**, 1092–1095 (2006).
7. R. P. A. Berntsson, L. Peng, L. M. Svensson, M. Dong, P. Stenmark, *Structure* **21**, 1602–1611 (2013).
8. R. P. A. Berntsson, L. Peng, M. Dong, P. Stenmark, *Nat. Commun.* **4**, 2058 (2013).
9. M. Dong *et al.*, *Science* **312**, 592–596 (2006).
10. L. Peng, W. H. Tepp, E. A. Johnson, M. Dong, *PLOS Pathog.* **7**, e1002008 (2011).
11. R. M. Benoit *et al.*, *Nature* **505**, 108–111 (2014).
12. K. Mann *et al.*, *EMBO J.* **8**, 65–72 (1989).
13. M. S. Ho, K. Böse, S. Mokkapati, R. Nischt, N. Smyth, *Microsc. Res. Tech.* **71**, 387–395 (2008).
14. J. Kruegel, N. Miosge, *Cell. Mol. Life Sci.* **67**, 2879–2895 (2010).
15. L. Dong *et al.*, *Lab. Invest.* **82**, 1617–1630 (2002).
16. A. Rummel, S. Bade, J. Alves, H. Bigalke, T. Binz, *J. Mol. Biol.* **326**, 835–847 (2003).
17. T. Binz, A. Rummel, *J. Neurochem.* **109**, 1584–1595 (2009).
18. C. Montecucco, *Trends Biochem. Sci.* **11**, 314–317 (1986).
19. A. Rummel *et al.*, *Proc. Natl. Acad. Sci. U.S.A.* **104**, 359–364 (2007).
20. M. A. Fox, M. S. Ho, N. Smyth, J. R. Sanes, *Neural Dev.* **3**, 24 (2008).
21. B. L. Bader *et al.*, *Mol. Cell. Biol.* **25**, 6846–6856 (2005).
22. S. Mahrhold, A. Rummel, H. Bigalke, B. Davletov, T. Binz, *FEBS Lett.* **580**, 2011–2014 (2006).
23. O. Suwan-apichon *et al.*, *Invest. Ophthalmol. Vis. Sci.* **47**, 133–139 (2006).
24. L. Restani *et al.*, *PLOS Pathog.* **8**, e1003087 (2012).
25. M. Matsuda, N. Sugimoto, K. Ozutsumi, T. Hirai, *Biochem. Biophys. Res. Commun.* **104**, 799–805 (1982).
26. F. L. Yeh *et al.*, *PLOS Pathog.* **6**, e1001207 (2010).
27. M. M. Martino *et al.*, *Science* **343**, 885–888 (2014).
28. L. Macri, D. Silverstein, R. A. Clark, *Adv. Drug Deliv. Rev.* **59**, 1366–1381 (2007).
29. E. Stryker, K. G. Johnson, *J. Cell Sci.* **120**, 3723–3728 (2007).
30. P. O'Grady, T. C. Thai, H. Saito, *J. Cell Biol.* **141**, 1675–1684 (1998).

ACKNOWLEDGMENTS

We thank S. Kjaer (Cancer Research UK London Research Institute) for help with the Octet RED96 system and K_d determination. N. O'Reilly and members of the Protein and Peptide Chemistry Laboratory (Cancer Research UK London Research Institute) for peptide synthesis, purification, and analysis; F. Giribaldi (Cancer Research UK London Research Institute) for help with footprint analyses; K. Deinhardt (University of Southampton) for mass spec analysis of axonal signaling endosomes; S. Swaminathan (Brookhaven National Laboratory) for experiments aiming at the crystallization of the N1 peptide-H_CT complex; A. Rummel and T. Binz (Medizinische Hochschule Hannover) and N. Fairweather (Imperial College London) for providing access to published H_CT mutants; I. Koxholt (University of Cologne) for help with nidogen-1 and -2 KO mice; and J. N. Sleigh (University College London) for help with statistical analyses. We also thank C. Montecucco (University of Padua) and S. Novoselov (University College London) for constructive comments. This work was supported by Cancer Research UK (K.B., N.S., M.G., M.W., and G.S.), by the Medical Research Council (M.W.), by the University of Padua (P.C. and G.Z.), and by the Deutsche Forschungsgemeinschaft (SFB 829) through the Collaborative Research Center at the University of Cologne and the "Köln Fortune Programm" (R.N.). L.G. is the Graham Watts Senior Research Fellow, supported by the Brain Research Trust. The data presented in this manuscript are found in the main paper and the supplementary data and materials and methods. The authors declare that they have no conflict of interest.

SUPPLEMENTARY MATERIALS

www.sciencemag.org/content/346/6213/1118/suppl/DC1
Materials and Methods
Figs. S1 to S9
Tables S1 to S4
References (*31*–*38*)
Movies S1 to S3

30 June 2014; accepted 5 November 2014
10.1126/science.1258138

T CELL SIGNALING

Antigen affinity, costimulation, and cytokine inputs sum linearly to amplify T cell expansion

Julia M. Marchingo,[1,2] Andrey Kan,[1,2] Robyn M. Sutherland,[1,2] Ken R. Duffy,[3] Cameron J. Wellard,[1,2] Gabrielle T. Belz,[1,2] Andrew M. Lew,[1,2] Mark R. Dowling,[1,2,4] Susanne Heinzel,[1,2]* Philip D. Hodgkin[1,2]*†

T cell responses are initiated by antigen and promoted by a range of costimulatory signals. Understanding how T cells integrate alternative signal combinations and make decisions affecting immune response strength or tolerance poses a considerable theoretical challenge. Here, we report that T cell receptor (TCR) and costimulatory signals imprint an early, cell-intrinsic, division fate, whereby cells effectively count through generations before returning automatically to a quiescent state. This autonomous program can be extended by cytokines. Signals from the TCR, costimulatory receptors, and cytokines add together using a linear division calculus, allowing the strength of a T cell response to be predicted from the sum of the underlying signal components. These data resolve a long-standing costimulation paradox and provide a quantitative paradigm for therapeutically manipulating immune response strength.

Upon infection, pathogen-specific $CD8^+$ T cells undergo a characteristic kinetic sequence: rapid proliferation and expansion followed by population contraction due to cell death (*1*). While short-term stimulation is sufficient to trigger $CD8^+$ T cell proliferation (*2*, *3*), further exposure to stimulatory signals is required for an effective response (*2*, *4*, *5*). Although multiple attempts have been made to create a theory relating the integration of stimulatory signals to T cell response strength, all have been qualitative (*6*) and thus have lacked the power to predict the quantitative effect of altering stimulatory combinations and strength. The current qualitative paradigm describes T cell activation and response magnitude as the outcome of three requisite signals: signal 1, T cell receptor (TCR) (*1*); signal 2, membrane-bound antigen-presenting cell (APC)–delivered costimuli (*4*); and signal 3, cytokines from inflammatory, homeostatic, or autocrine sources (*5*). The importance of these signals for T cell expansion is highly context-dependent, as classic in vitro studies have identified many "critical" signal 2 and 3 molecules (*5*, *7*–*9*); however, gene deletion typically yields only moderate defects in the in vivo $CD8^+$ T cell response (*10*–*13*), implying considerable redundancy.

Recent studies in B cells report an automated return to quiescence after a series of division rounds (*14*–*16*). The number of mitotic cycles B cells undergo varies and is influenced by the strength of stimulation. We hypothesized that T cells might be programmed in a similar manner with the final number of divisions (N) (Fig. 1A, left panel) a function of the sum of inputs from signals 1, 2, and 3 (illustrated in Fig. 1A). If correct, it may be possible to determine the calculus of addition to serve as the basis for a quantitative framework for T cell costimulation.

To test this hypothesis, we first measured the onset of quiescence in $CD8^+$ T cells using TCR-transgenic OT-I mice [which recognize chicken ovalbumin SIINFEKL (N4) peptide bound to $H2K^b$] crossed with FucciRG mice in which cells

[1]Division of Immunology, The Walter and Eliza Hall Institute of Medical Research, Parkville, VIC, Australia. [2]Department of Medical Biology, The University of Melbourne, Parkville, VIC, Australia. [3]Hamilton Institute, National University of Ireland, Maynooth, Ireland. [4]The Royal Melbourne Hospital, Parkville, VIC, Australia.
*These authors contributed equally to this work. †Corresponding author. E-mail: hodgkin@wehi.edu.au

fluoresce red (FucciR) during G_0/G_1 and green (FucciG) for the duration of the $S/G_2/M$ cell cycle phases (*17*). Quiescent ($FucciR^+G^-$), recently divided ($FucciR^-G^-$), and actively dividing ($FucciG^+$) cells can be distinguished, because cells that have reverted to a quiescent state (G_0) accumulate higher levels of FucciR (*17*, *18*). We define the number of generations of division before returning to quiescence as the cell's division destiny (DD) (*14*–*16*, *19*). OT-I/FucciRG $CD8^+$ T cells were transferred into mice infected with recombinant HKx31 influenza virus expressing N4 (HKx31-N4) (*20*). During early expansion, most OT-I/FucciRG $CD8^+$ T cells were proliferative, with <10% reverting to a quiescent state by day 3 of the response. This proportion of quiescent cells increased steadily, reaching ~75% of all OT-I/FucciRG $CD8^+$ T cells by the onset of contraction at day 7 (Fig. 1, B and C). To estimate the number of divisions T cells underwent before dropping out of cycle, the Cyton model (*15*, *21*) was fitted to total and quiescent cell numbers (Fig. 1D and table S1). Results were consistent with a T cell DD range spanning ~10 generations (Fig. 1E). If DD is carried through each cell lineage (*16*), this result predicts up to 1000-fold differences in T cell family size consistent with recent single-cell tracking studies (*22*, *23*).

To further explore the regulation of division progression, we developed a minimal in vitro stimulation system using CellTrace Violet (CTV)–labeled OT-I/FucciRG $CD8^+$ T cells. The contribution of signals 2 and 3 was reduced by using peptide self-presentation by purified $CD8^+$ T cells (*24*). The strong effect of autocrine interleukin-2 (IL-2) was controlled by adding blocking antibody (clone S4B6) and using human IL-2 (hIL-2), resistant to S4B6, when required (*25*). Superficially the in vitro pattern of early proliferation with a gradual onset of quiescence recapitulated the in vivo response (Fig. 1, C and F), with the major differences being the DD and subsequent time to die (Fig. 1, D, E, and G, and table S1).

We speculated that the three known sources of regulation—TCR affinity, costimuli, and cytokines—might combine to convert the low DD observed in vitro into the extensive outcome possible in vivo (Fig. 1E).

To improve estimation of mean DD (mDD) in our in vitro CTV division tracking assay, we used OT-I $CD8^+$ T cells deficient in the pro-apoptotic molecule Bim (OT-I/*Bcl2l11*$^{-/-}$) for all experiments. These cells reported the same mDD as OT-I/*Bcl2l11*$^{+/+}$ $CD8^+$ T cells (Fig. 2A; fig. S1, A to C; and table S2), but the enhanced survival upon reverting to quiescence facilitated DD measurement at later times, consistent with previous studies in B cells (*15*, *16*).

Fig. S2, A to F, shows the effect of a range of T cell stimuli on mDD. TCR affinity, several agonists representative of cell-contact–mediated costimulation, and some, but not all, cytokines tested were able to regulate DD in a dose-dependent manner. To determine when DD was most susceptible to regulation, cells from cultures where stimulation was removed immediately before the first division (*24*) were compared to cells with constant costimulation. Agonist antibodies to CD28 and CD27 principally acted before the first division. In contrast, ongoing exposure to IL-2, IL-4, and IL-12 was required for maximal proliferation (Fig. 2B). Higher levels of IL-2 or IL-4 caused T cells to divide beyond CTV resolution (fig. S3) and the culture capacity. Therefore, to investigate the potential of IL-2 and IL-4 to extend DD when cytokine levels were maintained, OT-I/*Bcl2l11*$^{-/-}$ $CD8^+$ T cells were subcultured every 48 hours in hIL-2 (Fig. 2C) or IL-4 (fig. S4A), and total cell numbers were calculated using splitting ratios. Cyton fitting revealed that hIL-2 and IL-4 can increase the mDD by up to ~11 and 7 divisions, respectively (Fig. 2, C to E; fig. S4, A and B; and tables S3 and S4). Titration of hIL-2 showed the effect on mDD to be dose dependent (Fig. 2D) and that this increase in mDD was associated with an increase in variance (Fig. 2E and fig. S4C). Together these results demonstrated that DD can be intrinsically programmed by early signals, but also has the flexibility to be "reprogrammed" or extended by extrinsic stimuli as the T cells divide.

We then determined how T cells integrated multiple contributors to DD. In Fig. 3, A and B, we show the increase in mDD imprinted before the first division for low concentrations of CD28 and CD27 agonist antibodies, and IL-12 protein. The combination of antibodies to CD28 and CD27 programmed an mDD that was equivalent to the sum of each individual effect, with IL-12 giving a slightly greater than additive increase in mDD

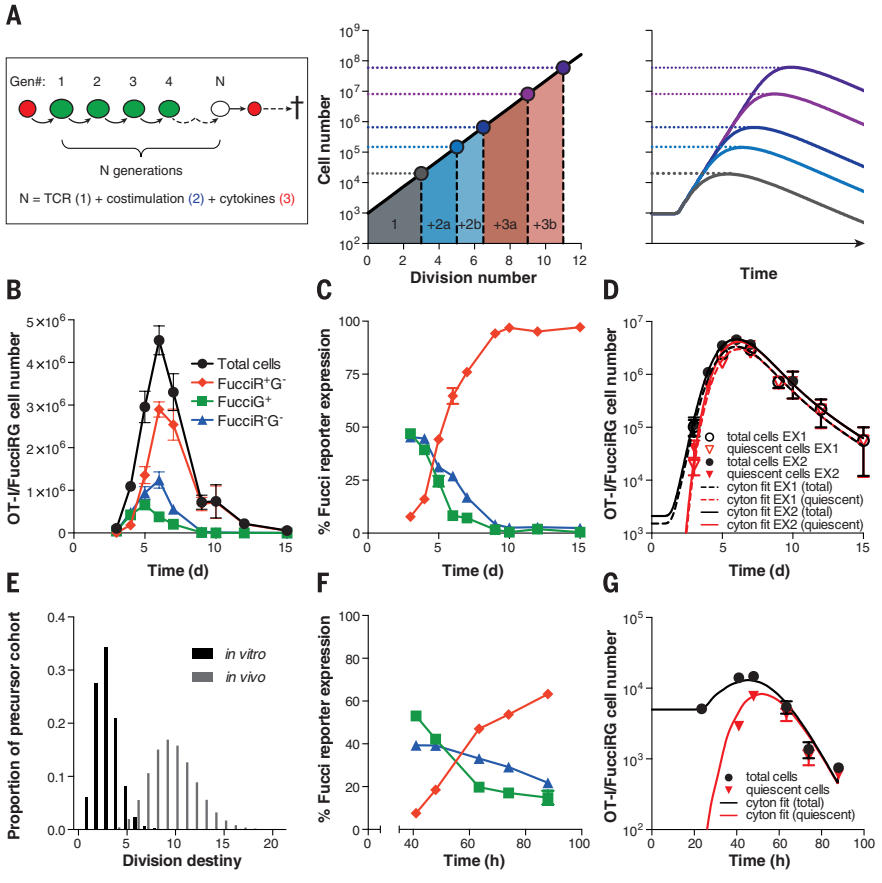

Fig. 1. $CD8^+$ T cells undergo a program of proliferation and quiescence in vivo and in vitro. (**A**) Quantitative T cell expansion hypothesis. By this model, the number of mitotic cycles a T cell undergoes after activation (N) varies and is determined by a sum of the individual inputs it receives. In the example shown, signal 1, 2, and 3 stimuli each individually elicit a small increase in mean population division number. The cumulative effect of these contributions, when summed linearly, would lead to geometric increases in total cell number at the peak response. Analysis of OT-I/FucciRG $CD8^+$ T cells [(B) to (E)] transferred to HKx31-N4–infected recipients on day 2 after infection or [(E) to (G)] in vitro stimulated with N4 in the presence of mIL-2 blocking antibody (S4B6). (**B**) Number and (**C**) percentage of OT-I/FucciRG $CD8^+$ T cells expressing FucciR and FucciG reporter proteins pooled from mediastinal lymph node, spleen, and lungs at the indicated time points after transfer. (**D**) Fitted total (black) and quiescent (red, $FucciR^+G^-$ + small $FucciR^-G^-$ cells) cell numbers using the Cyton model (*19*). (**E**) The estimated DD distribution from Cyton fitting to in vivo (D) and in vitro (G) stimulated cells. (**F**) Percentage of FucciR and FucciG expression. (**G**) Fitted total (black) and quiescent (red, $FucciR^+G^-$ + small $FucciR^-G^-$ cells) cell numbers (*19*). [(B) to (E)] n = 5 to 10 mice per time point, pooled from two independent experiments; mean ± SEM. [(E) to (G)] Representative of three independent experiments; mean ± SEM from triplicate culture wells.

(Fig. 3, C and D). Importantly, no single "second signal" appeared obligatory, but rather multiple small arithmetic effects on DD culminated in large geometric differences in the cell numbers produced (Fig. 1A, center and right panels). Thus, an increase of ~2.2 divisions in mDD (Fig. 3D) with the accompanying ~0.5 division increase in standard deviation (fig. S5, A to D, and table S5) summed from three weak costimuli resulted in a net ~8-fold increase in the peak cell number (Fig. 3, E and F), with the additional difference in response magnitude attributable to small variations in the starting cell number (fig. S5E and table S5). Early programming was cell intrinsic because cells imprinted with an mDD of ~1 or ~3.4 generations gave the same outcome irrespective of whether they were subsequently cultured separately or together (fig. S6, A and B). The approximately additive effect of stimuli on DD also applied for a range of combinations when stimuli were retained in culture during subsequent division rounds (fig. S7, A to D).

Taken together, this series of experiments reveals two stages of regulation of T cell DD. In the first stage, signal 1 and a series of signal 2 and 3 stimuli of different strengths and combinations can additively "program" a heritable number of division rounds before the first cell division. In the second stage, exposure to external signals, mainly cytokines, can be processed and added to the DD. These features are consistent with a molecular mechanism whereby each stimulatory signal contributes a quantum of mitosis-promoting

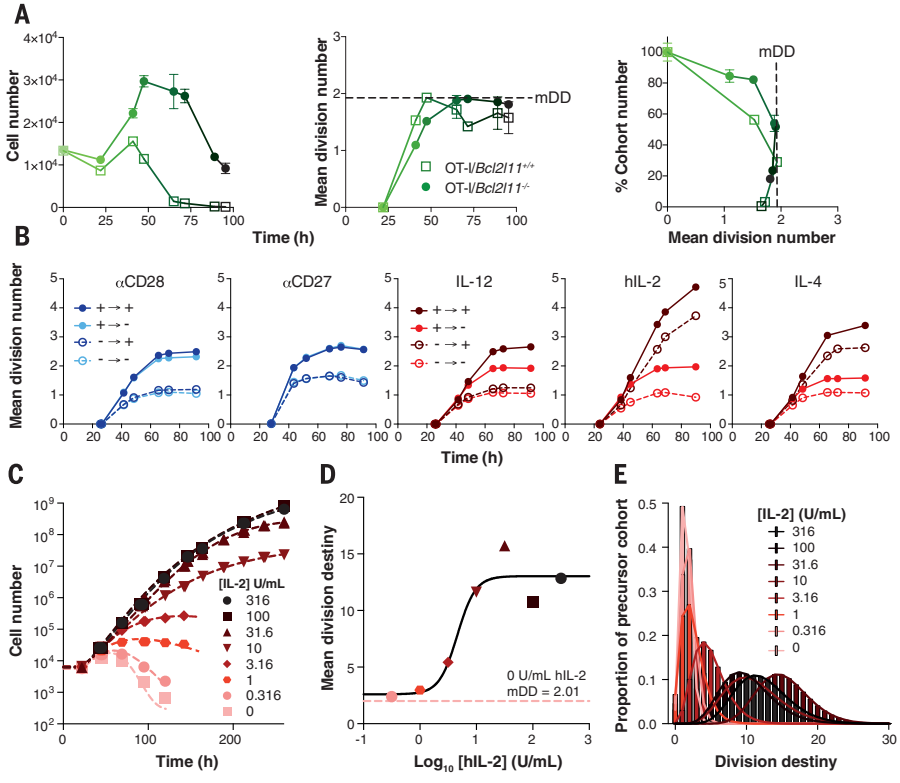

Fig. 2. Costimuli and cytokines program changes to DD. (**A**) CTV-labeled OT-I/*Bcl2l11*$^{+/+}$ or OT-I/*Bcl2l11*$^{-/-}$ CD8$^+$ T cells were stimulated with N4; total cell numbers (left), mean division number (middle), and an estimation of the percentage of the starting cells whose progeny are contributing to the response at that time point, calculated by removing the effect of cell expansion at each time point [percent cohort number, right; as described in (*19*)] were determined. Mean DD (mDD) on each graph is indicated by dotted lines. (**B**) Mean division number of CTV-labeled OT-I/*Bcl2l11*$^{-/-}$ CD8$^+$ T cells cultured in the presence (+, solid lines) or absence (−, dotted lines) of antibodies to CD28 (2 μg/mL) and CD27 (immobilized, 5 μg/mL) (blue), IL-12 (1 ng/mL), human IL-2 (hIL-2, 31.6 U/mL), or IL-4 (1000 U/mL) (red) for 26 hours, washed and further cultured with (dark) or without (light) costimulation. (**C**) CTV-labeled OT-I/*Bcl2l11*$^{-/-}$ CD8$^+$ T cells stimulated with N4 in the presence of hIL-2 at the indicated concentrations were subcultured into fresh hIL-2 every ~48 hours and the cell number was fitted using the Cyton model (dotted lines) (*19*). (**D** and **E**) Dose-response curve of mDD (D) and DD distributions (E) from Cyton fitting in (C). All cultures contained 25 μg/mL S4B6. Representative of at least two independent experiments; mean ± SEM from triplicate culture wells.

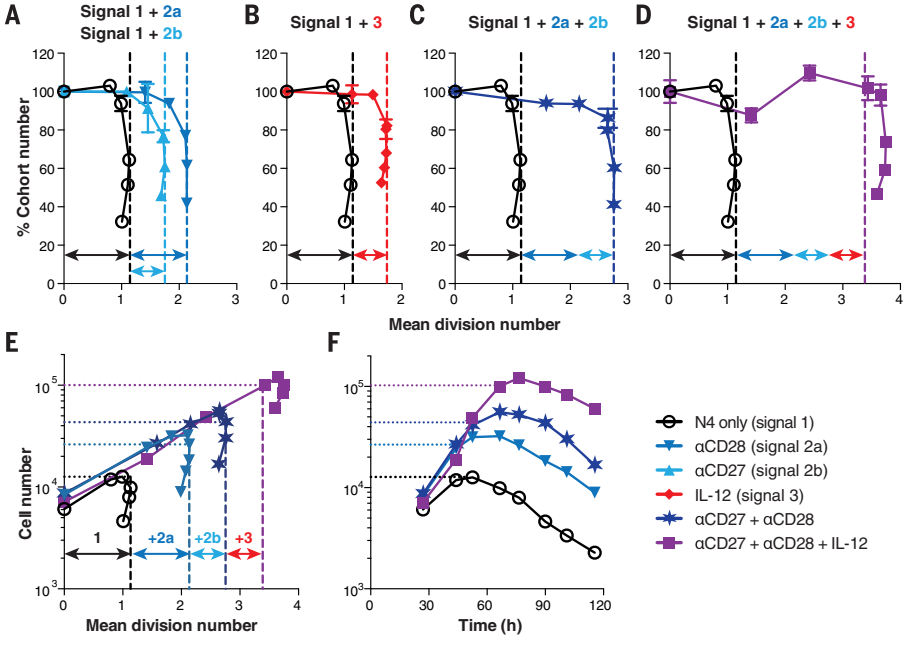

Fig. 3. Summation of DD from multiple costimuli geometrically amplifies the T cell response. Percentage cohort number (Fig. 2A) (*19*) versus mean division number for N4-stimulated, CTV-labeled OT-I/*Bcl2l11*$^{-/-}$ CD8$^+$ T cells cultured with (**A**) antibodies to CD27 (immobilized, 5 μg/mL) and CD28 (2 μg/mL) or (**B**) IL-12 protein (1 ng/mL) alone, (**C**) antibodies to CD27 and CD28 together, or (**D**) a combination of all three costimuli for 26 hours, washed and recultured without further stimulation. Relationship between cell number and either (**E**) mean division number or (**F**) time for data in [(A) to (D)]. Arrows represent the effect of individual stimuli on mDD. All cultures contained S4B6 at 25 μg/mL. Graphs are representative of three independent experiments; mean ± SEM of triplicate culture wells.

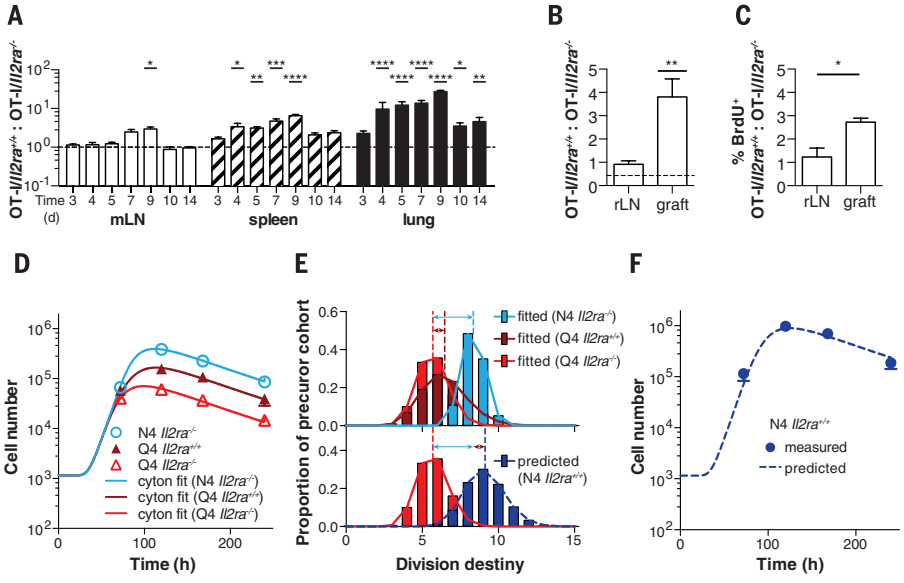

Fig. 4. In vivo summation of DD can predict T cell expansion. (**A**) Ratio of OT-I/*Il2ra*$^{+/+}$:OT-I/*Il2ra*$^{-/-}$ CD8$^+$ T cells recovered from mLN, spleen, and lungs after cotransfer of equal numbers of each into HKx31-N4–infected recipients. Mean ± SEM, n = 5 to 10 mice per time point, pooled from two independent experiments; two-way analysis of variance (ANOVA). (**B** and **C**) CTV-labeled OT-I/*Il2ra*$^{+/+}$ and OT-I/*Il2ra*$^{-/-}$ CD8$^+$ T cells were co-transferred to recipient mice at a 30:70 ratio 1 day before engraftment under the renal capsule with islets expressing membrane-bound ovalbumin under the rat insulin promoter. Mice were pulsed with BrdU 1 hour before organ harvesting on day 6 after engraftment, and the ratio of OT-I/*Il2ra*$^{+/+}$:OT-I/*Il2ra*$^{-/-}$ of (B) divided CD8$^+$ T cells and (C) the percentage of divided CD8$^+$ T cells positive for BrdU$^+$ within their respective genotype populations was measured in the renal (draining) lymph node (rLN) and graft. Mean ± SEM, n = 4 mice, representative of two independent experiments; two-way ANOVA and one-tailed t test, respectively. For all experiments, data points were excluded from ratio and percentage calculations when less than 100 cells were detected. Dotted lines in (A) and (B) represent the OT-I/*Il2ra*$^{+/+}$:OT-I/*Il2ra*$^{-/-}$ transfer ratio. (**D**) The Cyton model was fitted to OT-I/*Il2ra*$^{+/+}$ and OT-I/*Il2ra*$^{-/-}$CD8$^+$ T cell numbers from HKx31-Q4–infected mice and OT-I/*Il2ra*$^{-/-}$ CD8$^+$ T cells from HKx31-N4–infected mice pooled from the mLN, spleen, and lungs after cotransfer of equal numbers of cells into recipient mice, and (**E**) the division destiny distribution was determined (top) (*19*). By summation of mean and variance of these DD distributions, the cumulative effect of increasing TCR-antigen affinity and IL-2 signaling on the DD distribution (i.e., the DD distribution for OT-I/*Il2ra*$^{+/+}$ CD8$^+$ T cells in HKx31-N4–infected mice) was predicted (bottom). (**F**) Using this mean and variance, the cell number over time was predicted for OT-I/*Il2ra*$^{+/+}$ CD8$^+$ T cells in HKx31-N4–infected mice (*19*). Mean ± SEM; n = 5 mice per time point, representative of two independent experiments. ****P < 0.0001; ***P < 0.001; **P < 0.01; *P < 0.05.

protein or complex that is diluted by division until a submitotic concentration is reached and division ceases (*26*).

The two-stage DD programming model makes two key predictions for the role of extrinsic factors, such as IL-2, that could be tested during in vivo CD8$^+$ T cell responses: (i) the major physiological role of autocrine IL-2 is in maintaining division, and therefore it will be more important away from the initial site of CD8$^+$ T cell priming; and (ii) the effect of IL-2 on DD will sum with other stimuli, allowing the prediction of CD8$^+$ T cell expansion kinetics when IL-2 and other stimuli are combined.

We tested the first prediction by comparing the expansion of IL-2 receptor α–deficient OT-I CD8$^+$ T cells (OT-I/*Il2ra*$^{-/-}$) with OT-I/*Il2ra*$^{+/+}$ CD8$^+$ T cells in two different in vivo systems, namely an anti-influenza response and islet graft rejection model. Similar numbers of OT-I/*Il2ra*$^{+/+}$ and OT-I/*Il2ra*$^{-/-}$ CD8$^+$ T cells were detected at the site of priming [mediastinal lymph node (mLN)] during the expansion phase when cotransferred into HKx31-N4 infected mice (Fig. 4A). In contrast, a bias toward expansion of OT-I/*Il2ra*$^{+/+}$ CD8$^+$ T cells was observed in the spleen and lungs, consistent with a role for IL-2 in the maintenance of cell expansion (Fig. 4A). OT-I/*Il2ra*$^{+/+}$ CD8$^+$ T cells also outcompeted OT-I/*Il2ra*$^{-/-}$ CD8$^+$ T cells at the effector site during an anti-islet graft response (Fig. 4B). The proportion of bromodeoxyuridine-positive (BrdU$^+$) OT-I/*Il2ra*$^{+/+}$ CD8$^+$ T cells after a 1-hour in vivo BrdU pulse was ~2.5 times as high as for OT-I/*Il2ra*$^{-/-}$ CD8$^+$ T cells in the graft (Fig. 4C), confirming that this bias was attributable to proliferation in the effector site and not due to migration alone (*27*).

To investigate the additive nature of T cell stimuli in vivo, OT-I/*Il2ra*$^{+/+}$ and OT-I/*Il2ra*$^{-/-}$ CD8$^+$ T cells were cotransferred into mice infected with either high-affinity (HKx31-N4) or low-affinity (HKx31-Q4) influenza virus (*20*). The Cyton model was fitted to T cell numbers to estimate the increase in DD due to TCR affinity or IL-2 signaling alone (Fig. 4, D and E, top, and table S6). By summation of these individual contributions to the mean and variance of the DD distribution, we predicted the effect of a combined increase in TCR affinity and IL-2 signaling on DD (Fig. 4E, bottom) and successfully recreated the expansion kinetics of OT-I/*Il2ra*$^{+/+}$ CD8$^+$ T cells during an HKx31-N4 infection (Fig. 4F).

Manipulating T cell responses by costimulation and cytokine signaling is an important emerging therapeutic regimen (*28*, *29*), and a quantitative framework will facilitate the rational development of optimal interventions. To support this goal, we propose a quantitative paradigm where no one signal is obligatory but rather combinations of inputs add together to geometrically enhance outcomes (Fig. 1A). Thus, combinations of different costimulatory and cytokine signals provide many alternative paths to generate T cell responses of similar magnitude. This framework reconciles long-standing discrepancies between in vivo and in vitro results for IL-2 and costimulatory signals and reveals a quantitative basis for current switch-inspired two- and three-signal models of activation. Further studies measuring simultaneous differentiation changes to effector and memory states associated with cell division would complete the T cell calculating framework and further enhance our ability to predict therapeutic strategies for immunomodulation.

REFERENCES AND NOTES

1. D. Zehn, S. Y. Lee, M. J. Bevan, *Nature* **458**, 211–214 (2009).
2. S. M. Kaech, R. Ahmed, *Nat. Immunol.* **2**, 415–422 (2001).
3. M. J. van Stipdonk, E. E. Lemmens, S. P. Schoenberger, *Nat. Immunol.* **2**, 423–429 (2001).
4. E. M. Bertram, W. Dawicki, T. H. Watts, *Semin. Immunol.* **16**, 185–196 (2004).
5. J. M. Curtsinger *et al.*, *J. Immunol.* **162**, 3256–3262 (1999).
6. A. G. Baxter, P. D. Hodgkin, *Nat. Rev. Immunol.* **2**, 439–446 (2002).
7. D. A. Cantrell, K. A. Smith, *Science* **224**, 1312–1316 (1984).
8. L. A. Gravestein, J. D. Nieland, A. M. Kruisbeek, J. Borst, *Int. Immunol.* **7**, 551–557 (1995).
9. F. A. Harding, J. G. McArthur, J. A. Gross, D. H. Raulet, J. P. Allison, *Nature* **356**, 607–609 (1992).
10. T. R. Malek, *Annu. Rev. Immunol.* **26**, 453–479 (2008).
11. A. Oxenius, U. Karrer, R. M. Zinkernagel, H. Hengartner, *J. Immunol.* **162**, 965–973 (1999).
12. A. Shahinian *et al.*, *Science* **261**, 609–612 (1993).
13. K. P. J. M. van Gisbergen *et al.*, *Immunity* **35**, 97–108 (2011).
14. E. D. Hawkins, J. F. Markham, L. P. McGuinness, P. D. Hodgkin, *Proc. Natl. Acad. Sci. U.S.A.* **106**, 13457–13462 (2009).
15. E. D. Hawkins, M. L. Turner, M. R. Dowling, C. van Gend, P. D. Hodgkin, *Proc. Natl. Acad. Sci. U.S.A.* **104**, 5032–5037 (2007).
16. M. L. Turner, E. D. Hawkins, P. D. Hodgkin, *J. Immunol.* **181**, 374–382 (2008).
17. M. R. Dowling *et al.*, *Proc. Natl. Acad. Sci. U.S.A.* **111**, 6377–6382 (2014).
18. M. Tomura *et al.*, *PLOS ONE* **8**, e73801 (2013).
19. Materials and methods are available as supplementary materials on *Science* Online.
20. A. E. Denton *et al.*, *J. Immunol.* **187**, 5733–5744 (2011).
21. E. D. Hawkins *et al.*, *Nat. Commun.* **4**, 2406 (2013).
22. V. R. Buchholz *et al.*, *Science* **340**, 630–635 (2013).
23. C. Gerlach *et al.*, *Science* **340**, 635–639 (2013).
24. M. Hommel, P. D. Hodgkin, *J. Immunol.* **179**, 2250–2260 (2007).
25. E. K. Deenick, A. V. Gett, P. D. Hodgkin, *J. Immunol.* **170**, 4963–4972 (2003).
26. Because OT-I division times are relatively homogeneous, a division-based dilution model is difficult to distinguish from a mechanism where the loss of division motivation ceases in all

descendants at the same time after activation. Further molecular studies are needed to distinguish between these and other possible mechanisms.
27. W. Weninger, M. A. Crowley, N. Manjunath, U. H. von Andrian, *J. Exp. Med.* **194**, 953–966 (2001).
28. M. Dougan, G. Dranoff, *Annu. Rev. Immunol.* **27**, 83–117 (2009).
29. G. Kinnear, N. D. Jones, K. J. Wood, *Transplantation* **95**, 527–535 (2013).

ACKNOWLEDGMENTS

We thank S. Turner for providing the recombinant influenza virus and discussion and comments on the manuscript; L. Corcoran and V. Bryant for discussion and comments on the manuscript; A. Giang for discussion of experiments; M. Camilleri, L. Mackiewicz, M. Dayton, and D. Pavlyshyn for technical assistance; and P. Bouillet for *Bcl2l11*$^{-/-}$ mice. Fucci Red and Fucci Green mice were provided by the Riken BioResource Centre through the National BioResource Project of the Ministry of Education, Culture, Sports, Science, and Technology of Japan. We also thank K. Lafferty and his two-signal theory for inspiring this work. The data are tabulated in the main paper and in the supplementary materials. Experimental data and the code for fitting the Cyton model will be made available upon request. This work was supported by the National Health and Medical Research Council (NHMRC) through project grants 1010654 and 1043414, program grants 1054925 and 1037321, and fellowships to M.R.D., A.M.L., and P.D.H., K.R.D. and P.D.H. were supported by Human Frontier Science Program grant RGP0060/2012, G.T.B. was supported by an Australian Research Council Future Fellowship, and K.R.D. was supported by Science Foundation Ireland grant 12IP1263. This work was made possible through Victorian State Government Operational Infrastructure Support and Australian Government NHMRC Independent Research Institutes Infrastructure Support Scheme. J.M.M. was the recipient of an Australian Postgraduate Award and a Walter and Eliza Hall Institute Edith Moffat Scholarship.

SUPPLEMENTARY MATERIALS

www.sciencemag.org/content/346/6213/1123/suppl/DC1
Materials and Methods
Figs. S1 to S10
Tables S1 to S9
References (*30*–*32*)

15 August 2014; accepted 30 October 2014
10.1126/science.1260044

DNA REPAIR

Mechanism of DNA interstrand cross-link processing by repair nuclease FAN1

Renjing Wang,[1] Nicole S. Persky,[1] Barney Yoo,[2] Ouathek Ouerfelli,[2] Agata Smogorzewska,[3] Stephen J. Elledge,[4,5] Nikola P. Pavletich[1]*

DNA interstrand cross-links (ICLs) are highly toxic lesions associated with cancer and degenerative diseases. ICLs can be repaired by the Fanconi anemia (FA) pathway and through FA-independent processes involving the FAN1 nuclease. In this work, FAN1-DNA crystal structures and biochemical data reveal that human FAN1 cleaves DNA successively at every third nucleotide. In vitro, this exonuclease mechanism allows FAN1 to excise an ICL from one strand through flanking incisions. DNA access requires a 5′-terminal phosphate anchor at a nick or a 1- or 2-nucleotide flap and is augmented by a 3′ flap, suggesting that FAN1 action is coupled to DNA synthesis or recombination. FAN1's mechanism of ICL excision is well suited for processing other localized DNA adducts as well.

DNA interstrand cross-links (ICLs) covalently link together the two strands of the double helix (*1*). ICLs can be repaired by the Fanconi anemia (FA) pathway of proteins mutated in the FA cancer predisposition syndrome (*2*) and also by FA-independent processes (*1*, *3*, *4*). The FA pathway is activated when a replication fork stalls upon encountering an ICL, leading to unhooking of the ICL through flanking incisions on one strand, translesion DNA synthesis across the unhooked ICL, removal of the ICL remnants by additional incisions, and homologous recombination (*2*, *5*). The FAN1 nuclease (*6*–*9*) is a candidate for mediating FA-independent repair (*1*, *3*, *4*). Although FAN1 mutations result in defective ICL repair, chromosomal instability, and hypersensitivity to a wide range of ICL-inducing agents (*6*–*13*), they do not cause FA (*10*–*12*). Instead, they cause a kidney degeneration disorder known as karyomegalic interstitial nephritis (*11*). FAN1 cleaves branched DNA structures with a preference for 5′-flap substrates and also exhibits 5′- to 3′-exonuclease activity on a variety of double-stranded DNA (dsDNA) and single-stranded DNA (ssDNA) substrates (*6*–*9*). The functional implications of these broadly defined activities, whether FAN1 processes ICLs directly and in which manner, and the structural mechanism of ICL unhooking by nucleases are unknown.

To address these questions, we first investigated FAN1's DNA binding specificity for various lengths of 5′ flaps consisting of thymidine nucleotides (see supplementary materials and methods). We found that FAN1 exhibits specificity for a 5′ phosphate group at a flap of 1 to 2 nucleotides (nts) or at a nick, with dissociation constants (K_d) of 10.3 nM for the 1-nt flap (5′pT$_1$), 121 nM for 2 nts (5′pT$_2$), and 182 nM for the nick (pNi) (fig. S1A). The corresponding substrates lacking the 5′ phosphate group fail to bind appreciably until micromolar FAN1 concentrations (fig. S1A). Similarly, increasing the flap length beyond 2 nts reduces FAN1 affinity substantially (fig. S1A). We also tested the effect of adding a 3′ flap of eight thymidine nucleotides to the high-affinity 5′pT$_1$ (5′pT$_1$/3′T$_8$), 5′pT$_2$ (5′pT$_2$/3′T$_8$), and 5′pNi (5′pNi /3′T$_8$) and found that this increased their FAN1 affinity by a factor of ~25 to ~180 (K_d values of 0.4, 1.4, and 1.0 nM, respectively) (fig. S1B). By contrast, adding a 3′T$_8$ flap to the low-affinity 5′pT$_8$ (5′pT$_8$/3′T$_8$) minimally enhanced its affinity, with the resulting 377 nM K_d a factor of ~1000 weaker than that of 5′pT$_1$/3′T$_8$ (fig. S1B).

Based on these findings, we determined the 2.9 Å structure of a 5′pG$_1$/3′T$_4$ DNA bound to human FAN1 (residues 364 to 1017), N-terminally truncated to remove the ubiquitin-binding UBZ domain and subsequent unstructured segment, as well as the structure of apo-FAN1 (fig. S2A and table S1). FAN1 has a bilobal structure consisting of a 223-residue N-terminal domain (NTD) and a 415-residue C-terminal domain (CTD) that contains the PD-(D/E)XK nuclease motif (Fig. 1, A and B). The DNA adopts a V-shaped structure, with a kink at the nick. The prenick and postnick duplexes have an overall B-form DNA (B-DNA) conformation, with a 76° angle between them. The prenick duplex and 3′ flap are bound by the NTD, whereas the 5′ flap and postnick duplex are bound by the CTD. There are no major conformational changes between the apo- and DNA-bound FAN1 structures (fig. S2B).

The NTD consists of a helical domain, a winged-helix DNA binding domain, and the predicted SAP domain (Fig. 1C). These form a continuous surface that binds to a 9–base pair duplex segment leading to the 3′ flap and to a 2-nt segment of the flap (Fig. 1A and fig. S3, A to D). The duplex contacts involve only phosphodiester groups (fig. S3, A to D), except for the flap-proximal base pair, which is contacted at both its phosphodiester and base groups (Fig. 2A). These base contacts block the DNA from extending as a regularly stacked duplex, analogous to the helix-breaking wedges observed with other structure-specific nucleases (*14*, *15*).

Only the first two nucleotides of the 3′T$_4$ flap are ordered. These extend away from the duplex and are bound by FAN1 (Fig. 2A). The base and ribose groups of the first nucleotide are contacted by Tyr^{374}, Val^{577}, and Arg^{581}. The phosphate group

[1]Structural Biology Program and Howard Hughes Medical Institute, Memorial Sloan Kettering Cancer Center, New York, NY 10065, USA. [2]Molecular Pharmacology and Chemistry Program, Memorial Sloan Kettering Cancer Center, New York, NY 10065, USA. [3]Laboratory of Genome Maintenance, The Rockefeller University, New York, NY 10065, USA. [4]Department of Genetics and Howard Hughes Medical Institute, Harvard Medical School, Boston, MA 02115, USA. [5]Division of Genetics, Brigham and Women's Hospital, Boston, MA 02115, USA.
*Corresponding author. E-mail: pavletin@mskcc.org

Editor's Summary

Stimulatory signals add up for T cells

T cell activation is a dynamic process. T cells encounter multiple input signals such as antigens, costimulatory molecules, and cytokines at different times and anatomical locations during an infection. But how do T cells integrate this information to determine the extent to which they divide? To find out, Marchingo *et al.* stimulated mouse T cells in culture with different combinations of inputs and also tracked antigen-specific T cell responses in mice infected with influenza virus. They found that T cells linearly sum the various stimulatory inputs they receive to determine their "division destiny."

Science, this issue p. 1123